AIMS Mathematics, 10(5): 10387–10412.
DOI: 10.3934/math.2025473
Received: 02 January 2025
Revised: 03 April 2025
Accepted: 15 April 2025
Published: 06 May 2025

https://www.aimspress.com/journal/Math

Research article

Intelligent neural networks approach for analysis of the MHD viscous nanofluid flow due to rotating disk with slip effect

Yousef Jawarneh[1], Samia Noor[2,3,*], Ajed Akbar[4], Rafaqat Ali Khan[4] and Ahmad Shafee[5]

[1] Department of Mathematics, College of Science, University of Ha'il, Ha'il 2440, Saudi Arabia; Email: y.jawarneh@uoh.edu.sa
[2] Department of Basic Sciences, General Administration of Preparatory Year, King Faisal University, P.O. Box 400, Al Ahsa 31982, Saudi Arabia
[3] Department of Mathematics and Statistics, College of Science, King Faisal University, P.O. Box 400, Al Ahsa 31982, Saudi Arabia
[4] Department of Mathematics, Government Postgraduate College Nowshera, Khyber Pakhtunkhwa, Pakistan, Email: ajedakbar@gmail.com, rafimaths957@gmail.com
[5] PAAET, College of Technological Studies, Laboratory Technology Department, Shuwaikh 70654, Kuwait; Email: As.zada@paaet.edu.kw

* **Correspondence:** Email: snoor@kfu.edu.sa.

Abstract: This analysis used the backpropagation Levenberg-Marquardt technique coupled through neural networks (BPLMT-NN). The magnetohydrodynamic (MHD) viscous nanofluid flow due to the rotating disk (MHD-VNRD) through the slip effect was investigated. In the existence of a velocity slip condition, this communication investigated the boundary coating flow of viscous nanofluid under MHD conditions. The flow was produced by a disk that was revolving. A fluid effects electricity under the effect of a magnetic field that is transverse. The magnetic field that is generated is neglected when the magnetic Reynolds number is low. The properties of Brownian and thermophoresis motion were demonstrated using a nanofluid simulation. Hypotheses about the boundary coating and low magnetic Reynolds number were made while formulating the problem. To transform nonlinear partial differential equations into a scheme of ordinary differential equations, the similarity transformation was utilized. On the profiles of velocity, temperature, and concentration, a data set for the suggested (BPLMT-NN) was created for the impacts of several important parameters and was illustrated via the explicit Runge-Kutta technique. Using the (BPLMT-NN) testing, training, and validation approach, the estimated result of various situations was endorsed, and the suggested model was evaluated for fitness. After that, the proposed (BPLMT-NN) was validated using mean square error (MSE),

regression analysis, and histogram investigations. The novelty of the proposed BPLMT-NN technique has various applications, such as disease diagnosis, robotic control systems, ecosystem evaluation, etc. We conducted analyses of some statistical data like gradient, performance, and epoch of the proposed fluid model. Based on closeness, as well as recommended and reference results, the suggested approach has made a distinction with precision level varying from 10^{-09} to 10^{-1} .

Keywords: nanoparticles; magnetic field; rotating disk; velocity slip; neural network; Levenberg-Marquard technique
Mathematics Subject Classification: 34G20, 35R11

Nomenclature

MHD	Magnetohydrodynamic	D_T	Thermophoretic diffusion coefficient $[m^2s^{-1}]$
Ω	Angular velocity $[ms^{-1}]$	L	Velocity slip constant $[ms^{-1}]$
B_0	Magnetic field strength $[NmA^{-1}]$	T_w	Temperatures of the surface
(u, v, w)	Velocity components $[ms^{-1}]$	T_∞	Temperatures for away from the surface
(r, ϕ, z)	Cylindrical coordinates $[m]$	C_w	Concentration at the surface
v	Kinematic viscosity $[m^2s^{-1}]$	C_w	Concentration for away from the surface
μ	Dynamic viscosity $[kgm^{-1}s^{-1}]$	η	Similarity variable
ρ_f	Density of base fluid $[kg\ m^{-3}]$	M	Magnetic parameter
σ	Electrical conductivity $[Sm^{-1}]$	γ	Velocity slip parameter
T	Temperature of fluid $[K]$	Pr	Prandtl number
α	Thermal diffusivity of fluid $[m^2s^{-1}]$	Nb	Brownian motion parameter
k	Thermal conductivity of fluid $[Wm^{-1}K^{-1}]$	Nt	Thermophoresis parameter
$(\rho c)_f$	Heat capacity of fluid $[JK^{-1}]$	Le	Lewis number
$(\rho c)_p$	Heat capacity of nanoparticles $[JK^{-1}]$	Re_r	Local rotational Reynolds number
D_B	Brownian diffusion coefficient $[m^2s^{-1}]$	f'	Dimensionless velocities
C	Concentration	g	Dimensionless velocities
ANN	Artificial neural networks	ϕ	Concentration distribution
MSE	Mean square error	θ	Temperature field
BPLMT	Backpropagation Levenberg Marquardt technique		

1. Introduction

Neural networks are widely utilized, having applications in enterprise planning, financial

operations, trading, product maintenance and business analytics. Neural networks are also widely used in corporate applications such as marketing exploration and forecasting, risk assessment, and fraud detection. Backpropagation is a popular learning process in input multilayer neural networks. This approach has lately been employed by researchers to investigate mass and heat transfer characteristics, as well as non-Newtonian fluid flow systems. In 1974 Paul Werbos was the foremost person to design the backpropagation technique. This method was revived and improved upon by Rumelhart and Parker [1] after Paul Werbos's discovery. An artificial neural network (ANN) is an innovative new artificial intelligence method. ANNs can exploit a variety of disciplines throughout the learning development depending on the data that flows through the network, whether it initiates from inside or outside of it. To enhance the multilayer perceptron (MLP) network's performance, an ANN uses the back propagation technique for simultaneous training. It is the most widely used, easy-to-learn, and successful model for complex multilayer networks. A unique convergent consistency technique for ANNs is the Levenberg-Marquardt technique (LMT), which provides a numerical solution to a range of fluid flow issues. Various researchers have lately utilized this technique to analyze non-Newtonian fluid flow systems and their properties related to mass and heat transfer. In their study, Ajed et al. [2] suggested using neural network design to inspect the heat transfer and MHD in a two-phase paradigm of nanofluid flow when thermal energy exists. Over a stretched sheet, Shoaib et al. [3] examined the numerical analysis for rotational MHD nanofluid flow hybrids with heat radiation using neural networks. Utilizing the back-propagated neural networks with Levenberg-Marquard system (BNN-LMS), Khan et al. [4] investigated the heat transfer across two porous parallel surfaces of stable nanofluids utilizing thermophoresis and Brownian effects. Using a backpropagation Levenberg-Marquardt, Sabir et al. [5] studied methods of computational intelligence to clarify the Emden-Fowler paradigm's third-order nonlinear scheme. Shafiq et al. [6] explored the modeling of Soret and Dufour's convective heat transfer in nanofluid flow through a moving needle with an artificial neural network. Shoaib et al. [7] exercised the technique of Levenberg–Marquardt back propagation with neural networks (TLMB-NN) and a stochastic numerical approach via ANNs to study the consequences of heat transfer on Maxwell flow of nanofluid above a vertical moving surface with MHD. Intelligent networks were utilized by Ajed et al. [8] to study MHD flow of fluid in a thermally stratified medium across coaxial extensible spinning disks. Sindhu et al. [9] investigated the reliability study of generalized exponential distribution based on inverse power law using an artificial neural network with Bayesian regularization.

To compare the performance of different neural network models for robustness verification, we need to consider various factors such as the type of verification, the size and complexity of the network, and the robustness metric used [10].

Types of verification:

i) Point-wise verification
ii) Partition-based verification

Alternative neural network models:

i) Deep neural networks (DNNs)
ii) Convolutional neural networks (CNNs)

Performance comparison:

Efficiency: Partition-based verification can be more efficient than point-wise verification, especially for large networks.

Accuracy: The accuracy of robustness verification depends on the robustness metric used and the quality of the partitioning in partition-based verification.

Scalability: DNNs and CNNs can be computationally expensive to verify, especially for large

networks. Partition-based verification can help improve scalability.

Researchers are working harder than ever in applied physics and engineering to improve and understand the valuable properties of nanomaterials. The past few years have seen a surge in interest in nanofluids [11,12]. The extreme heat conductivity of microfluids sets them apart from ordinary fluids. The enhancement in thermal conductivity of nanofluids has overtaken the restricted transfer of heat performance of conventional fluids currently in use as an extremely important phenomenon. Researchers are drawn to the exciting and crucial analysis of nanofluids because of the potential uses, for instance safer surgery, electrical gadgets, cancer therapy and nuclear reactors may boost heat transfer resources for a better cooling method, Nayak et al. [13]. Choi and Eastman et al. [14] seemed to be the initial researchers to report the dispersion of nanoparticles in a base fluid in 1995. Sheikholeslami et al. [15] studied the features of nanofluids, such as viscosity, conductivity, and thermal property, which have a substantial influence on heat transfer rates. There is now a large body of work on the mixed convection nanofluid flow stagnation points. Syam et al. [16] investigated the dynamics of Fe_3O_4–water, Cu–water, and Ag–water nanofluids in the context of steady, two-dimensional, incompressible laminar magnetohydrodynamic (MHD) boundary layer flow. Makinde et al. [17] explored the influence of the magnetic field and buoyancy pressure at a conduction-heated medium on the stagnation point flows. Metals, carbides, oxides, and carbon nanotubes are often discovered to include nanoparticles. In the fields of biomedicine, computer microprocessors, nuclear reactor cooling, and industry, nanofluids are broadly exploited to enhance the heat transfer [18,19]. Syam et al. [20] investigated the slip flow dynamics involving Al_2O_3 and Fe_3O_4 nanoparticles within a horizontal channel embedded with porous media. Nadeem et al. [21] investigated a unique kind of nanofluid; they found that the nanoparticles could have been tabular or rod-shaped.

The flow caused by disk rotation is currently of much curiosity because of its extensive range of uses in engineering and aeronautical science branches, for example, medical apparatus, thermal power-producing systems, rotating equipment, computer-storing tools, gas turbine blades, crystal growth methods, etc. Von Karman [22] pioneered the flow caused by a revolving disk. His well-known work has been explored by many scholars throughout the world through varied approaches. Turkyilmazoglu and Senel [23] investigated a combined impact of heat and mass transfer phenomena in the rotating flow of a viscous fluid over a permeable disk. They analyzed the numerical outcomes of the flow problem. Rashidi et al. [24] investigated the MHD viscous fluid flow via a spinning disk with various parameters. In this research, they also looked at how entropy creation affected the flow of the problem under consideration. Turkyilmazoglu [25] presented on the flow of a revolving disk while taking nanoparticle impacts into consideration. Hatami et al. [26] investigated the laminar, incompressible viscous nanoliquid flow produced by revolving and compressing disks. They performed the study using the smallest squares approach. Mustafa et al. [27] have studied the flow caused by a linear extending disk in the existence of nanoparticles. They came to the conclusion that a major factor in lowering the thickness of the boundary coating is the uniform stretching of the disk. Sheikholeslami et al. [28] reported the numerical solutions for the nanofluid flow issue affected by an angled spinning disk.

Currently, increased heat transmission rates are required by industrial production processes. The appropriate heat transfer rates required by industry are not being fulfilled by the traditional heat transfer technologies. The main focus of contemporary scientists working on this topic is the development of methods for improving heat transmission. Enhancement methods may be broadly divided into two groups: Active as well as passive procedures. While active methods need external forces like magnetic and electric fields, passive techniques just require certain fluid extracts, thermal packing, geometries, etc. Enhancing the thermal execution of common liquids, including water, oil,

and ethylene-glycol combinations is the main goal of fluid additives [29]. Numerous researchers have documented how solid-liquid mixtures significantly increase heat transmission. Various problems have been identified as the reason why this combination was not suitable for improving thermal performance, including clogging, abrasion, and increased pressure loss.

There has been a lot of importance in the analysis of MHD boundary coating flow and heat transfer in recent years because of its applications in engineering and technology. Initially, astrophysical and geophysical problems were resolved with MHDs. Among its many applications were in silk drift separation, drug delivery, biomedicine, optical modulators, magnetic cell separation, optical grids, and optical switches, and nonlinear optical materials. MHDs are concerned with the flow of an electrically behaving fluid in a magnetic field, which has the power to regulate system flow and heat transfer. In 1974 the MHD boundary coating flow of an electrically affecting fluid in the existence of a constant transverse magnetic field was investigated by Pavlov et al. [30]. Gupta and Chakrabarti et al. [31] built on this work by observing MHD flow and heat transfer in 1979. When a magnetic field was introduced, Hayat et al. [32] observed the MHD flow of Sisko nanofluid and hypothesized that the bidirectional stretching of the surface was the cause of the flow production. Heysiattalab et al. [33] inspected the anisotropic action of magnetic nanofluids throughout film-wise condensing across a vertical plate with a constant variable-directional magnetic field. Hayat et al. [34] investigate the MHD three-dimensional nanofluid flow via a nonlinear stretching surface that had been convectively heated. Hayat et al. [35] investigated the stratified flow of a thixotropic nanofluid in the presence of magnetic field effects. Malvandi et al. [36] investigated the thermal properties of hydromagnetic nanofluid flow in a vertical micro annular tube. Hayat et al. [37] have presented an analytical approach for the three-dimensional Oldroyd-B nanofluid flow with heat generation and preoccupation. Examining the mean hydrodynamic drag (MHD) of a viscous nanoliquid as a result of a spinning disk is the main objective of this study. Interactions between nanoparticles cause Brownian motion and thermophoretic phenomena. We applied the velocity slip scenario instead of the no-slip requirement. Very often, velocity slip may occur between the moving surface and the fluid when the liquid in question is particulate, as is the case with rarefied gas, suspensions, mixes, and so on. In these cases, the slip condition, which is defined by Navier's equation, determines the proper boundary condition.

Investigator employ a pattern of numerical and semi-numerical methods to solve problems when getting a precise analytical resolve may be challenging. Methodologies include spectral relaxation [38], the HAM method [39], the Galerkin finite element method [40], the Keller box method [41], and many others. Evolutionary approximation approaches have been employed in stochastic numerical computing algorithms linked to neural networks to identify the solutions/outcomes of differential equations for both linear and nonlinear cases, showing separate evaluations for different parameters. Thermodynamics [42], magnetohydrodynamics [43,44], COVID-19 models [45,46], nanotechnology [47], mosquito dispersal models [48], flow model of micro polar nanofluid flow [49], Emden Fowler systems [50,51], nonlinear corneal shape models [52] and atomic physics [53] are among the methodologies that are used.

By analyzing the effects of all alterations or physical measurements on profiles of velocity, concentration, and temperature, and exploiting numerical and graphical studies, these compelling characteristics encourage researchers to exploit a reputable and precise AI algorithm-based numerical computational framework for numerical investigation of the MHD nanofluid mathematical model. MATLAB and Mathematica both were operated to improve numerical performance.

The innovation contributions of the present study for backpropagation networks for the magnetohydrodynamic nanofluid flow due to the rotating disk (MHD-VNRD) model are highlighted as follows.

- The numerical computation has been designed through the neural networks with the backpropogation Levenberg-Marquardt scheme (BPLMT-NN) for the comparative study of the impact of magnetohydrodynamic nanofluid flow over a rotating disk (MHD-VNRD) with slip effects.
- The governing mathematical model of the impact of magnetohydrodynamic nanofluid flow over a rotating disk (MHD-VNRD) with slip effects represented with nonlinear PDEs is reduced to a nonlinear system of ODEs by the competency of similarity adjustments.
- Reference data of designed networks is constructed effectively for variants of MHD-VNRD demonstrating the scenarios for the velocity slip parameter, parameter of Brownian motion, magnetic field parameter, Prandtle number, thermophoresis parameter, and Lewis number by applying the RK4 method.
- Mathematica software is used to compute the dataset for designed BPLMT-NN for the variation of the velocity slip parameter, the parameter of Brownian motion, magnetic field parameter, Prandtle number, thermophoresis parameter, and Lewis number.
- MATLAB software is used to interpret the solution and the absolute error analysis plots of MHD-VNRD.
- The training, testing, and validation-based process block structure of BPLMT-NN exploited to calculate the approximate solutions of MHD-VNRD and comparative study validate the consistent accuracy.
- The worthy performance of the designed network was additionally established by the learning curve on MSE-based fitness, histograms, and regression metrics.

The study has been organized as follows:

The purpose and implications of the MHD-VNRD paradigm are discussed in Section 2. The solution methodology and the impact of the suggested BPLMT-NN on many MHD-VNRD alternatives are covered in Section 3. The findings evaluation is covered in Section 4, and some last thoughts and suggestions for future study are contained in Section 5.

2. Mathematical interpretation and evaluation of flow

We study the steady-state MHD boundary coating flow caused by a rotating disk under the condition of velocity slip, resulting in an incompressible viscous nanofluid with $z = 0$, and the disk rotating with an angular velocity Ω, which is constant. When a homogeneous magnetic field of intensity B_0 is employed in a certain direction, a viscous fluid conducts electricity (see Figure 1). Also, the electric field and Hall current are not taken into consideration. A low magnetic Reynolds number has no bearing on the generated magnetic field. Aspects of heat transfer and mass are studied when Brownian motion and thermophoresis are present. The directions of escalating (r, φ, z) correspond to the velocity components (u, v, w). According to [25,28], the following boundary coating expressions control the current flow state:

$$\frac{\partial u}{\partial r}+\frac{u}{r}+\frac{\partial w}{\partial z}=0, \tag{1}$$

$$u\frac{\partial u}{\partial r}-\frac{v^2}{r}+w\frac{\partial u}{\partial z}=\nu\left(\frac{1}{r}\frac{\partial u}{\partial r}-\frac{u}{r^2}+\frac{\partial^2 u}{\partial r^2}+\frac{\partial^2 u}{\partial z^2}\right)-\frac{B_0^2\sigma}{\rho_f}u, \tag{2}$$

$$u\frac{\partial v}{\partial r}+\frac{uv}{r}+w\frac{\partial v}{\partial z}=(\frac{1}{r}\frac{\partial v}{\partial r}-\frac{v}{r^2}+\frac{\partial^2 v}{\partial r^2}+\frac{\partial^2 v}{\partial z^2})\nu-\frac{\sigma B_0^2}{\rho_f}v, \tag{3}$$

$$u\frac{\partial w}{\partial r}+w\frac{\partial w}{\partial z}=\left(\frac{\partial^2 w}{\partial r^2}+\frac{1}{r}\frac{\partial w}{\partial r}+\frac{\partial^2 w}{\partial z^2}\right)\nu, \tag{4}$$

$$u\frac{\partial T}{\partial r}+w\frac{\partial T}{\partial z}=\alpha\left(\frac{1}{r}\frac{\partial T}{\partial r}+\frac{\partial^2 T}{\partial r^2}+\frac{\partial^2 T}{\partial z^2}\right)+\frac{(\rho c)_p}{(\rho c)_f}\left[\left(\frac{\partial T}{\partial r}\frac{\partial C}{\partial r}+\frac{\partial T}{\partial z}\frac{\partial C}{\partial z}\right)D_B+\left(\left(\frac{\partial T}{\partial r}\right)^2+\left(\frac{\partial T}{\partial z}\right)^2\right)\frac{D_T}{T\infty}\right], \tag{5}$$

$$u\frac{\partial C}{\partial r}+w\frac{\partial C}{\partial z}=D_B\left(\frac{1}{r}\frac{\partial C}{\partial r}+\frac{\partial^2 C}{\partial r^2}+\frac{\partial^2 C}{\partial z^2}\right)+\frac{D_T}{T_\infty}\left(\frac{\partial^2 T}{\partial r^2}+\frac{1}{r}\frac{\partial T}{\partial r}+\frac{\partial^2 T}{\partial z^2}\right). \tag{6}$$

The related boundary conditions are

$$\begin{aligned} &u=L\frac{\partial u}{\partial z},\ \ v=\Omega r+L\frac{\partial v}{\partial z},\ \ w=0,\ T=T_w,\ C=C_w\ \ as\ z\to 0,\\ &u\to 0,\ \ v\to 0,\quad T\to T_\infty,\ C\to C_\infty\quad as\ \ z\to\infty \end{aligned}. \tag{7}$$

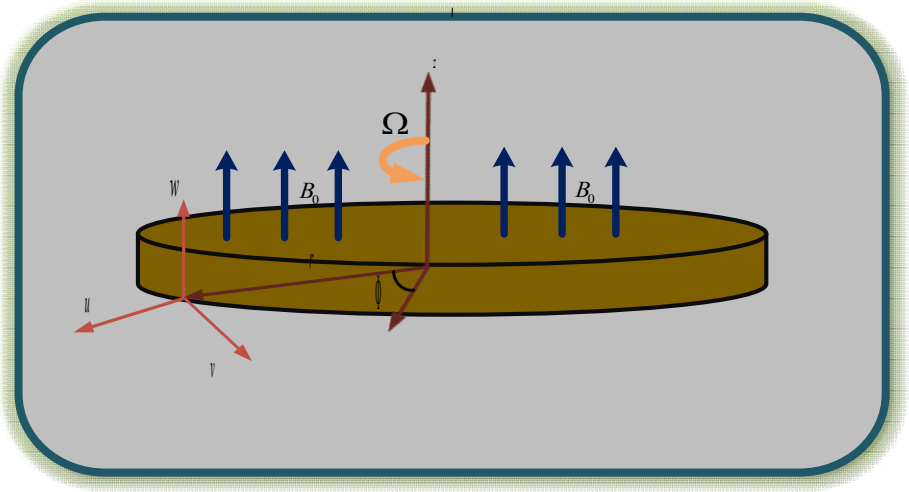

Figure 1. The MHD-VNRD flow geometry.

Where μ represents the dynamic viscosity, ρ_f denotes the density of base fluid, $\nu\ (=\frac{\mu}{\rho_f})$ the kinematic viscosity, σ is the electrical conductivity, $\alpha=\frac{k}{(\rho_c)_f}$ denotes the thermal diffusivity of fluid, T is the temperature, k represents the thermal conductivity of fluid, $(\rho_c)_p$ is the effective heat capacity of nanoparticles, $(\rho_c)_f$ is the heat capacity of fluid, D_B is the coefficient of the Brownian diffusion, D_T denotes the coefficient of the thermophoretic diffusion, C is the concentration, L is the velocity slip constant, C_w shows the concentration at the surface C_∞ represents the concentration far from the surface T_w shows the temperature at the surface, and T_∞ represents the temperature far from the surface.

The subsequent dimensionless variables are now introduced:[54]

$$v = r\Omega g^{'}(\eta),\ u = r\Omega f^{'}(\eta),\ w = -(2\Omega\nu)^{1/2} f(\eta),$$
$$\phi(\eta) = \frac{C - C_\infty}{C_w - C_\infty},\ \ \theta(\eta) = \frac{T - T_\infty}{T_w - T_\infty},\ \ \ \eta = (\frac{2\Omega}{\nu})^{1/2} z. \tag{8}$$

Now Eq (1) is fulfilled and Eqs (2)–(7) become to the subsequent structures:

$$2f^{'''} + 2ff^{''} - (f^{'})^2 - M^2 f^{'} + g^2 = 0, \tag{9}$$

$$2g^{''} + 2g^{'} f - 2f^{'} g - M^2 g = 0, \tag{10}$$

$$\theta^{''} + \Pr(Nb\theta^{'}\phi^{'} + f\theta^{'} + Nt\theta^{'2}) = 0, \tag{11}$$

$$\phi^{''} + \frac{Nt}{Nb}\theta^{''} + \Pr Le\, f\phi^{'} = 0. \tag{12}$$

The converted boundary conditions are defined as:

$$f = 0,\ f' = rf''(0),\ \ g' = 1 + \gamma g''(0),\ \ \theta = 1,\ \ \ \phi = 1\ \ at\ \eta = 0,$$
$$g = 0,\ f' = 0,\ \ \varphi = 0, \theta = 0\ \ at\ \eta \to \infty. \tag{13}$$

Here γ denotes the parameter of velocity slip, M is the magnetic parameter, the Prandtl number is represented by Pr, Nt is the thermophoresis parameter, Le is the Lewis number, and Nb is the parameter of the Brownian motion. All the parameters are expressed as follows:

$$M^2 = \frac{\sigma B_0^2}{\rho_f \Omega}, \gamma = L\sqrt{\frac{2\Omega}{\nu}}, Nb = \frac{(\rho c)_p}{(\rho c)_f}\frac{(T_w - T_\infty)}{T_\infty \nu},$$
$$Le = \frac{\alpha}{D_B}, \Pr = \frac{\nu}{\alpha}, Nt = \frac{(\rho c)_p}{(\rho c)_f}\frac{(C_w - C_\infty)}{\nu}. \tag{14}$$

The non-dimensional kind of skin friction coefficients and local Nusselt and Sherwood values can be found as

$$(\mathrm{Re}_r)^{1/2} C_f = f^{''}(0),$$
$$(\mathrm{Re}_r)^{1/2} C_g = g^{'}(0). \tag{15}$$

3. Methodology and evaluation

In Figure 2, the proposed BPLMT-NN is displayed within a neural network. Using 'nftool', a method for fitting a neural network in MATLAB, the suggested BPLMT-NN is achieved. Levenberg-Marquardt backpropagation is utilized to find the weight of neural networks.

The suggested BPLMT-NN approach is shown in Figure 3, while Figure 4 shows a single flow diagram that illustrates the whole study process. Using 'nftool', six different MHD-VNRD model variants are analyzed; BPLMT-NN provides the correct solution.

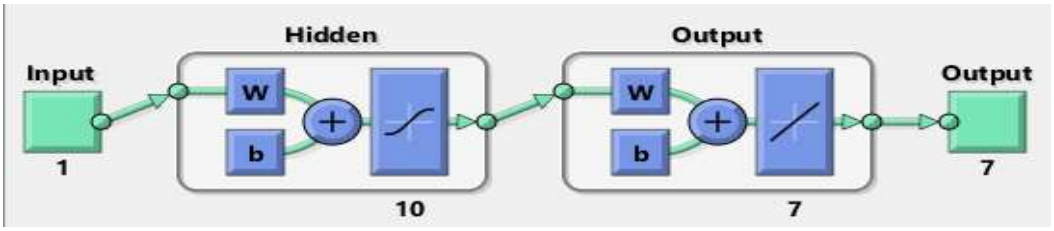

Figure 2. The MHD-VNRD model's neural network architecture.

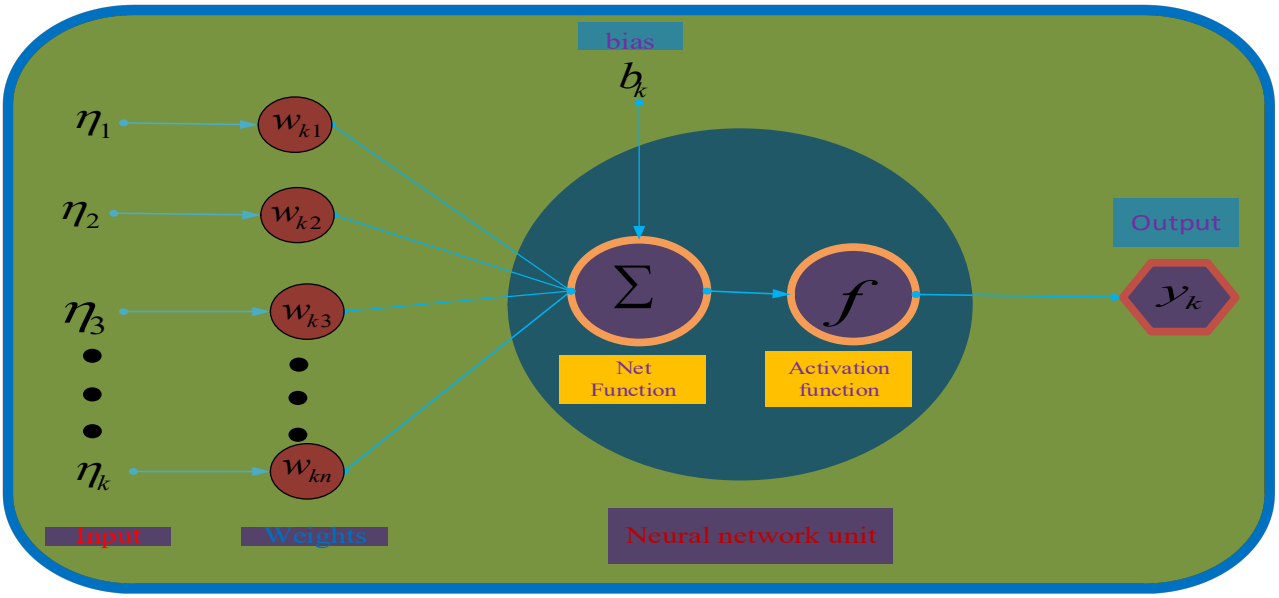

Figure 3. The structure of a particular neuron type.

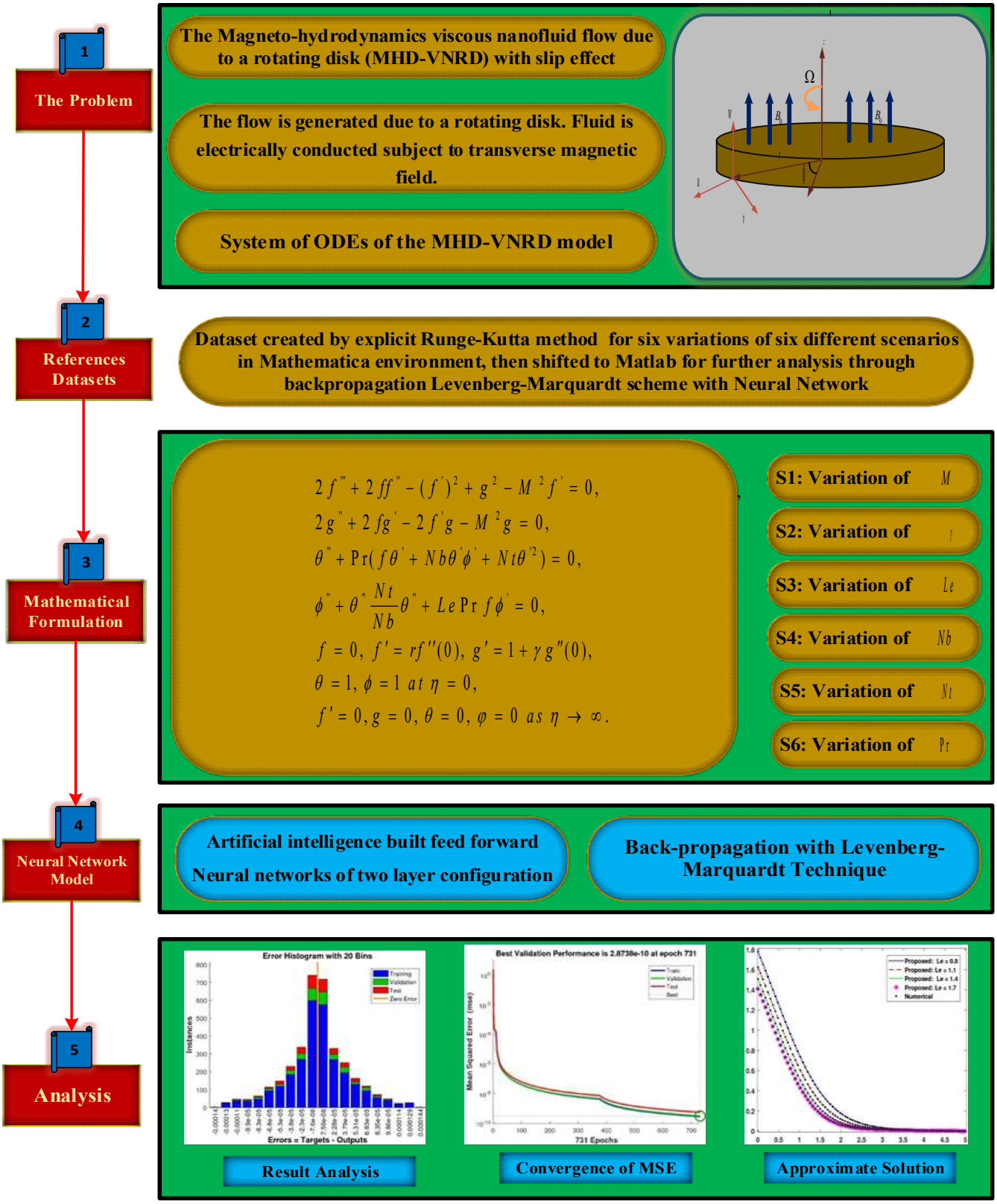

Figure 4. The workflow method for BPLMT-NN that is applied for the MHD-VNRD model.

Figures 5–8 show how the BPLMT-NN affects the MHD-VNRD model for Scenarios 1–6. The error histogram, fitting, and MSE performance diagrams for each of the six Case 4 scenarios $M, \gamma, Le, Nb, Nt,$ and Pr are displayed in Figures 5(i) and 5(ii). Figures 6(i) and 6(ii) show the state transitions and regression analysis for all of the four MHD-VNRD model cases. Table 1 display

illustration of four separate cases and all six MHD-VNRD model scenarios, while Tables 2 and 3 display the convergence achieved parameters for Case 4 of Scenarios 1–6 in the form of executed period, performance duration, backpropagation, MSE, execution, and sequential complicated gauges.

Table 1. Illustration of four separate cases and all six MHD-VNRD model scenarios.

Case	Physical quantities are present in interest-based scenarios					
	M	γ	Le	Nb	Nt	Pr
C1	0.0	0.2	1.0	0.5	0.2	1.2
C2	0.4	0.2	1.0	0.5	0.2	1.2
C3	0.7	0.2	1.0	0.5	0.2	1.2
C4	1.0	0.2	1.0	0.5	0.2	1.2
C1	0.2	0.2	1.0	0.5	0.2	1.2
C2	0.2	0.4	1.0	0.5	0.2	1.2
C3	0.2	0.6	1.0	0.5	0.2	1.2
C4	0.2	0.8	1.0	0.5	0.2	1.2
C1	0.2	0.2	0.8	0.5	0.2	1.2
C2	0.2	0.2	1.1	0.5	0.2	1.2
C3	0.2	0.2	1.4	0.5	0.2	1.2
C4	0.2	0.2	1.7	0.5	0.2	1.2
C1	0.2	0.2	1.0	0.3	0.2	1.2
C2	0.2	0.2	1.0	0.6	0.2	1.2
C3	0.2	0.2	1.0	0.9	0.2	1.2
C4	0.2	0.2	1.0	1.2	0.2	1.2
C1	0.2	0.2	1.0	0.5	0.0	1.2
C2	0.2	0.2	1.0	0.5	0.3	1.2
C3	0.2	0.2	1.0	0.5	0.6	1.2
C4	0.2	0.2	1.0	0.5	1.0	1.2
C1	0.2	0.2	1.0	0.5	0.2	0.7
C2	0.2	0.2	1.0	0.5	0.2	1.0
C3	0.2	0.2	1.0	0.5	0.2	1.3
C4	0.2	0.2	1.0	0.5	0.2	1.6

The MSE evolutions, training, and validation convergences for Scenarios 1–6 of the MHD-VNRD model are shown in Subfigures 5(i) and 5(ii) with regard to testing procedures. The suggested approach performs more accurately and efficiently when the MSE value is lower. With MSE close to $1.24 \times 10^{-10}, 2.61 \times 10^{-10}, 1.93 \times 10^{-09}, 2.58 \times 10^{-10}, 7.09 \times 10^{-10}$, and 3.16×10^{-11}, the greatest network performance is achieved.

The produced results of six distinct scenarios with a step size of 0.01 and inputs ranging from 0 to 5 are examined in Figures 5(i)–5(ii) to illustrate the effectiveness of the MHD-VNRD model. By connecting the obtained results to explicit Runge-Kutta technique reference numerical results and related results, the error dynamics plot is validated. The error histograms in Figures 5(i)–5(ii) are just one part of the study. The MHD-VNRD model's error dynamics and results for Case 4 of different situations are also looked at for all input points. It was found that the suggested BPLMT-NN has a maximum error of less than 1.85×10^{-10}, 5.08×10^{-10}, 2.00×10^{-09}, 2.76×10^{-10}, 8.53×10^{-10} and 1.66×10^{-05} for Case 4 of the figures 1to 6 scenarios of the design model. For point 4 of

the Figures 1 to 6 various scenarios of MHD-VNRD, the error bin average value relative to the zero line has error near -3.3×10^{-06}, 1.01×10^{-05}, -7.6×10^{-06}, 4.53×10^{-06}, -7.42×10^{-06}, and -2.2×10^{-06}. In relation to the values of the Levenberg-Marquardt gradient and step size of Mu, the following values are strongly related: $[1.00 \times 10^{-08}, 1.00 \times 10^{-08}, 1.00 \times 10^{-08}, 1.00 \times 10^{-08}, 1.00 \times 10^{-08}, \text{and } 1.00 \times 10^{-085}]$ and $[9.97 \times 10^{-08}, 9.96 \times 10^{-08}, 9.99 \times 10^{-0}, 9.99 \times 10^{-08}, 9.96 \times 10^{-0}, \text{and } 9.97 \times 10^{-08}]$ are displayed in Subfigures 6(i) and 6(ii). BPLMT-NN is competent, dependable, and convergent, as demonstrated by the outcomes and graphical depictions for the MHD-VNRD model in Case 4. Corelation analyses are frequently used to classify data in regression analysis. The correlation R values exhibit a consistent proximity to one, indicating optimality for testing, training, and validation in certain modeling scenarios. This indicates the MHD-VNRD model resolution of the BPLMT-NN. Furthermore, as in 4 of the several MHD-VNRD model Scenarios 1–6, the corresponding numerical values in Tables 2 and 3 show that the MSE performance for the recommended BPLMT-NN is close to 10^{-11}. Tables 2 and 3's numerical results demonstrate how well the BPLMT-NN executes the MHD-VNRD model.

Table 2. Consequences of the BPLMT-NN for the MHD-VNRD model for Scenarios 1–3.

Scenario	Case	Mean Square Error			Execution	Gradient	Mu	Epoch	Time
		Training	Validation	Testing					
S1	1	1.64700×10^{-10}	1.90753×10^{-10}	1.68195×10^{-10}	1.65×10^{-10}	9.96×10^{-08}	1.0×10^{-08}	41	03
	2	3.16411×10^{-10}	3.70464×10^{-10}	3.23186×10^{-10}	3.16×10^{-10}	9.96×10^{-08}	1.0×10^{-08}	808	06
	3	2.10645×10^{-11}	1.81508×10^{-11}	2.16156×10^{-11}	2.11×10^{-11}	9.96×10^{-08}	1.0×10^{-09}	334	02
	4	1.24179×10^{-10}	1.85570×10^{-10}	1.29493×10^{-10}	1.24×10^{-10}	9.97×10^{-08}	1.0×10^{-08}	446	03
S2	1	1.83756×10^{-10}	2.87199×10^{-10}	1.73325×10^{-10}	1.64×10^{-10}	9.99×10^{-08}	1.0×10^{-08}	397	03
	2	1.68052×10^{-10}	1.98824×10^{-10}	1.68488×10^{-10}	1.68×10^{-10}	9.99×10^{-08}	1.0×10^{-08}	746	05
	3	1.78484×10^{-11}	3.71330×10^{-11}	1.77313×10^{-11}	1.78×10^{-11}	9.96×10^{-08}	1.0×10^{-09}	382	02
	4	2.61293×10^{-10}	2.87381×10^{-10}	5.08270×10^{-10}	2.61×10^{-10}	9.96×10^{-08}	1.0×10^{-08}	731	05
S3	1	1.59733×10^{-09}	1.57392×10^{-09}	3.00322×10^{-09}	1.60×10^{-09}	9.92×10^{-08}	1.0×10^{-08}	329	02
	2	1.47057×10^{-09}	1.48823×10^{-09}	1.50023×10^{-09}	1.47×10^{-09}	9.98×10^{-08}	1.0×10^{-08}	393	03
	3	1.82443×10^{-09}	1.96767×10^{-09}	2.30347×10^{-09}	1.82×10^{-09}	9.96×10^{-08}	1.0×10^{-08}	447	03
	4	1.92974×10^{-09}	2.00536×10^{-09}	1.91311×10^{-09}	1.93×10^{-09}	9.99×10^{-08}	1.0×10^{-08}	405	03

Table 3. Consequences of the BPLMT-NN for the MHD-VNRD model for Scenarios 4–6.

Scenario	Case	MSE			Execution	Gradient	Mu	Epoch	Time
		Training	Validation	Testing					
S4	1	1.86338×10^{-10}	2.13947×10^{-10}	2.14676×10^{-10}	1.86×10^{-10}	9.98×10^{-08}	1.0×10^{-08}	421	03
	2	1.53546×10^{-10}	1.65814×10^{-10}	1.54422×10^{-10}	1.54×10^{-10}	1.00×10^{-07}	1.0×10^{-08}	425	03
	3	1.87084×10^{-10}	1.86256×10^{-10}	1.95960×10^{-10}	1.87×10^{-10}	9.96×10^{-08}	1.0×10^{-08}	444	03
	4	2.57696×10^{-10}	2.75791×10^{-10}	2.38404×10^{-10}	2.58×10^{-10}	9.99×10^{-08}	1.0×10^{-08}	480	03
S5	1	5.51350×10^{-10}	7.16027×10^{-10}	8.37695×10^{-10}	5.51×10^{-10}	9.96×10^{-08}	1.0×10^{-08}	354	02
	2	4.63292×10^{-10}	1.79700×10^{-09}	8.90578×10^{-10}	4.63×10^{-10}	9.95×10^{-08}	1.0×10^{-08}	453	03
	3	6.73531×10^{-10}	7.60358×10^{-10}	7.12512×10^{-10}	6.74×10^{-10}	9.99×10^{-08}	1.0×10^{-08}	361	03
	4	7.09104×10^{-10}	7.79336×10^{-10}	8.53258×10^{-10}	7.09×10^{-10}	9.96×10^{-08}	1.0×10^{-08}	354	03
S6	1	1.96004×10^{-11}	5.08381×10^{-11}	1.56826×10^{-11}	1.96×10^{-11}	9.99×10^{-08}	1.0×10^{-09}	289	02
	2	1.78326×10^{-10}	2.93967×10^{-10}	2.06403×10^{-10}	1.78×10^{-10}	9.95×10^{-08}	1.0×10^{-08}	401	03
	3	1.75126×10^{-10}	1.96179×10^{-10}	2.09772×10^{-10}	1.75×10^{-10}	9.98×10^{-08}	1.0×10^{-08}	482	04
	4	3.16448×10^{-11}	2.88223×10^{-11}	3.17947×10^{-11}	3.16×10^{-11}	9.97×10^{-08}	1.0×10^{-08}	350	03

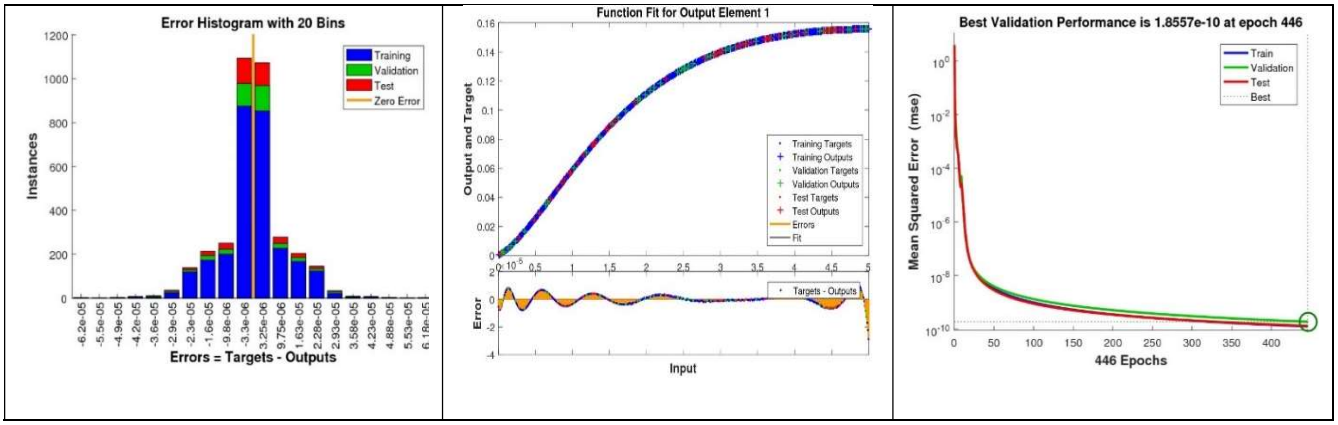

(a) Effects of the error histogram, fitness, and MSE performance for Scenario S1, Case C4.

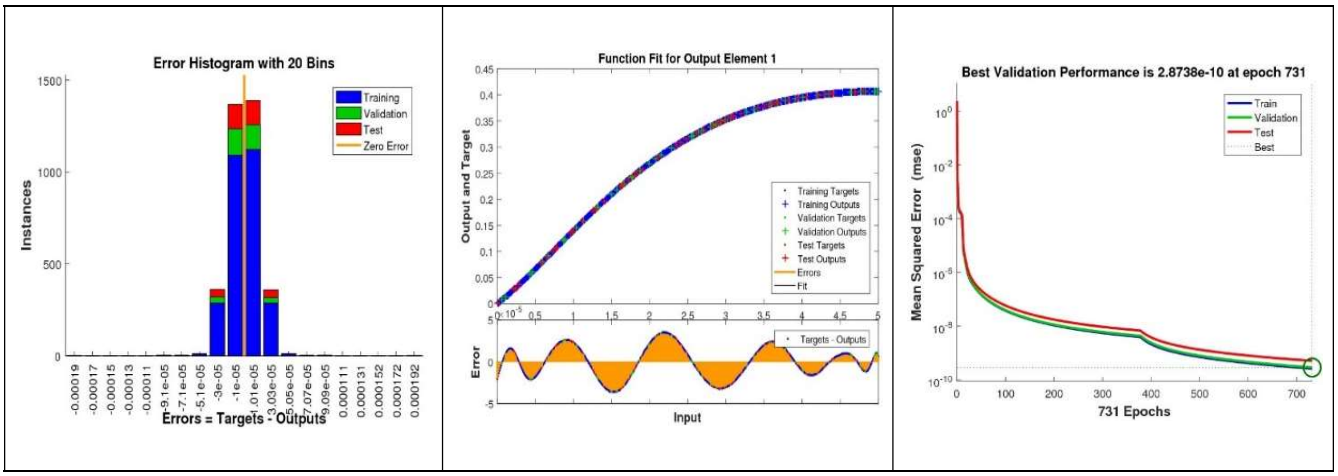

(b) Effects of the error histogram, fitness, and MSE performance for Scenario S2, Case C4.

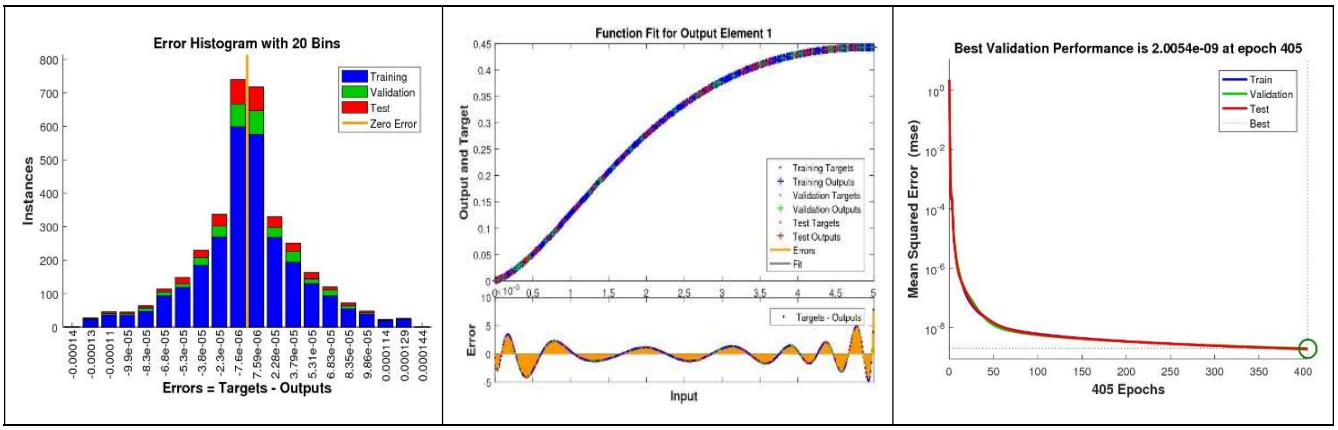

(c) Effects of the error histogram, fitness, and MSE performance for Scenario S3, Case C4.

Figure 5(i). Suggested BPLMT-NN error histogram, performance, and fitness solutions for solving Case 4 of Scenarios 1–3 in the MHD-VNRD model.

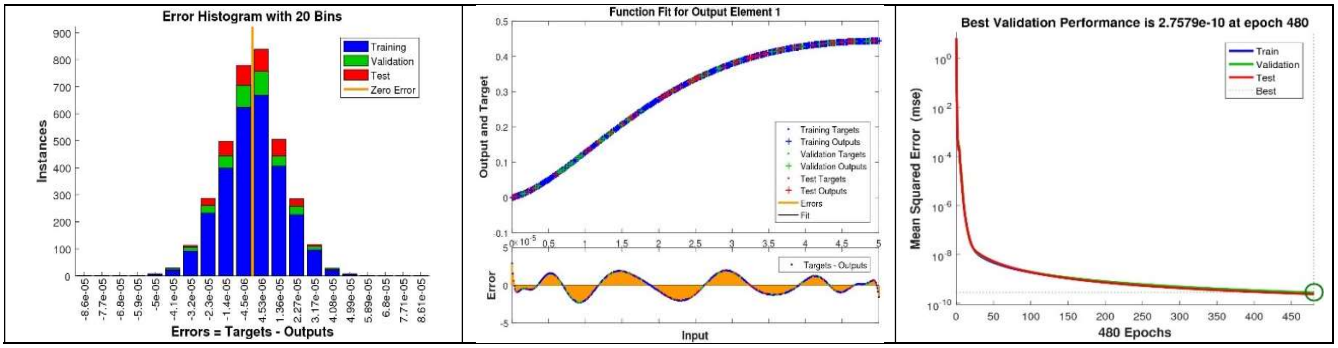

(a) Effects of the error histogram, fitness, and MSE performance for Scenario S4, Case C4.

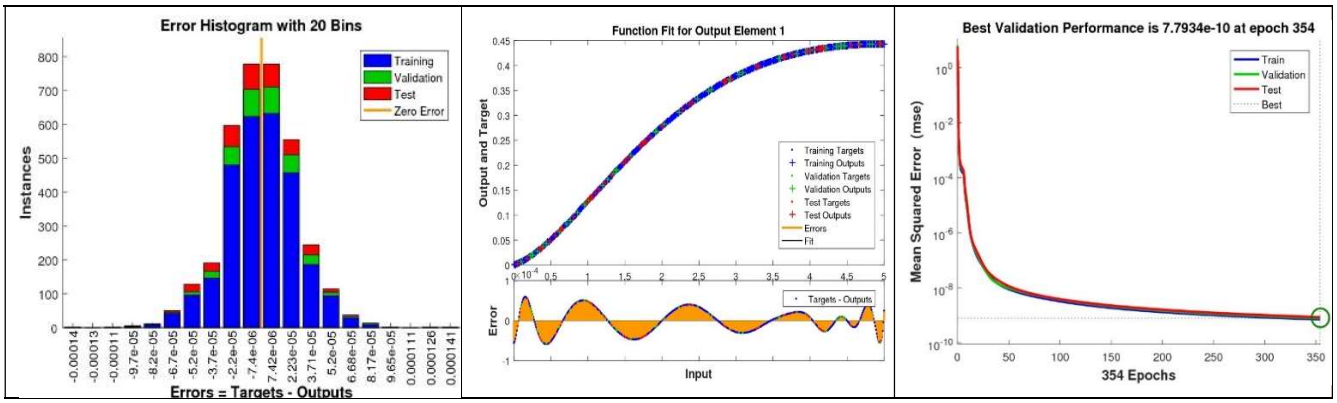

(b) Effects of the error histogram, fitness, and MSE performance for Scenario S5, Case C4.

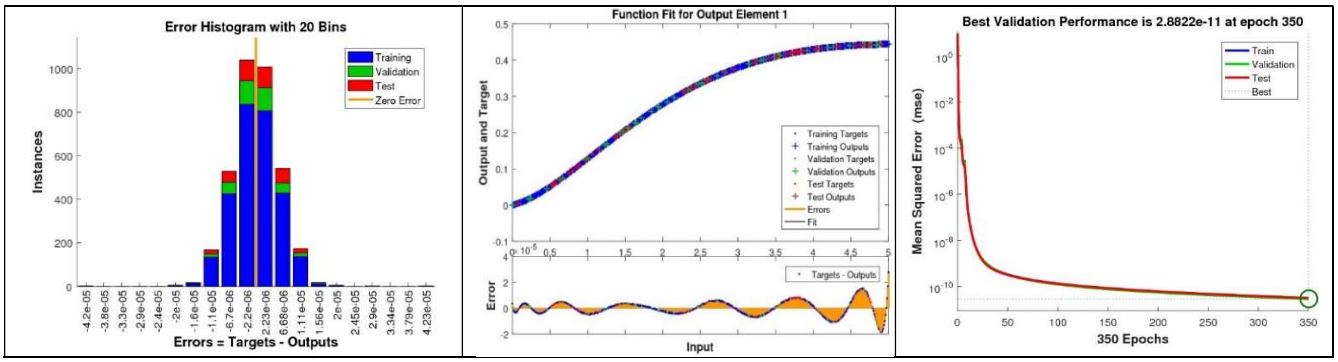

(c) Effects of the error histogram, fitness, and MSE performance for Scenario S6, Case C4.

Figure 5(ii). Suggested BPLMT-NN error histogram, performance, and fitness solutions for solving Case 4 of Scenarios 4–6 in the MHD-VNRD model.

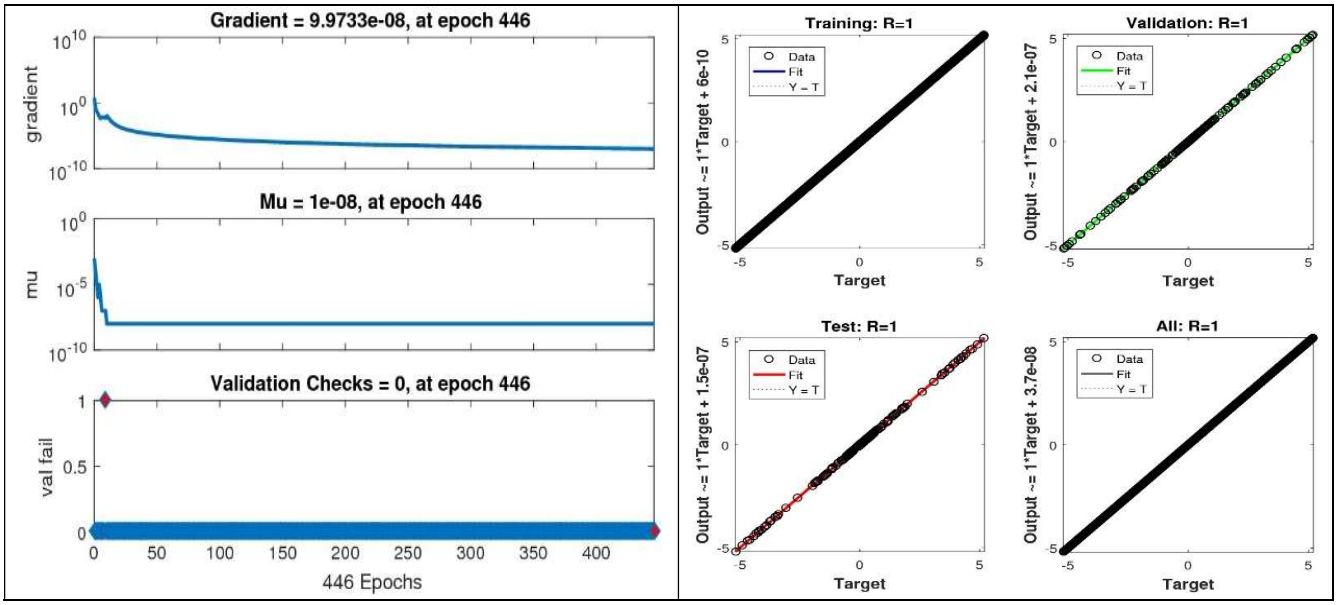

(a) State transition and regression analysis results for S1 of C4.

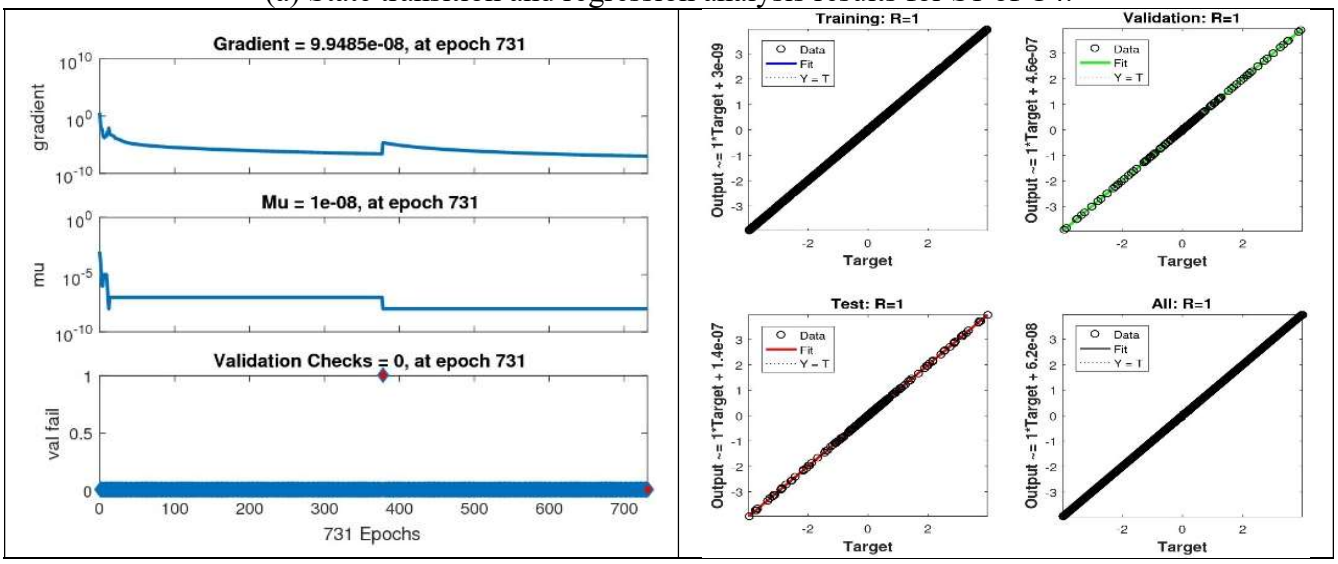

(b) State transition and regression analysis results for S2 of C4.

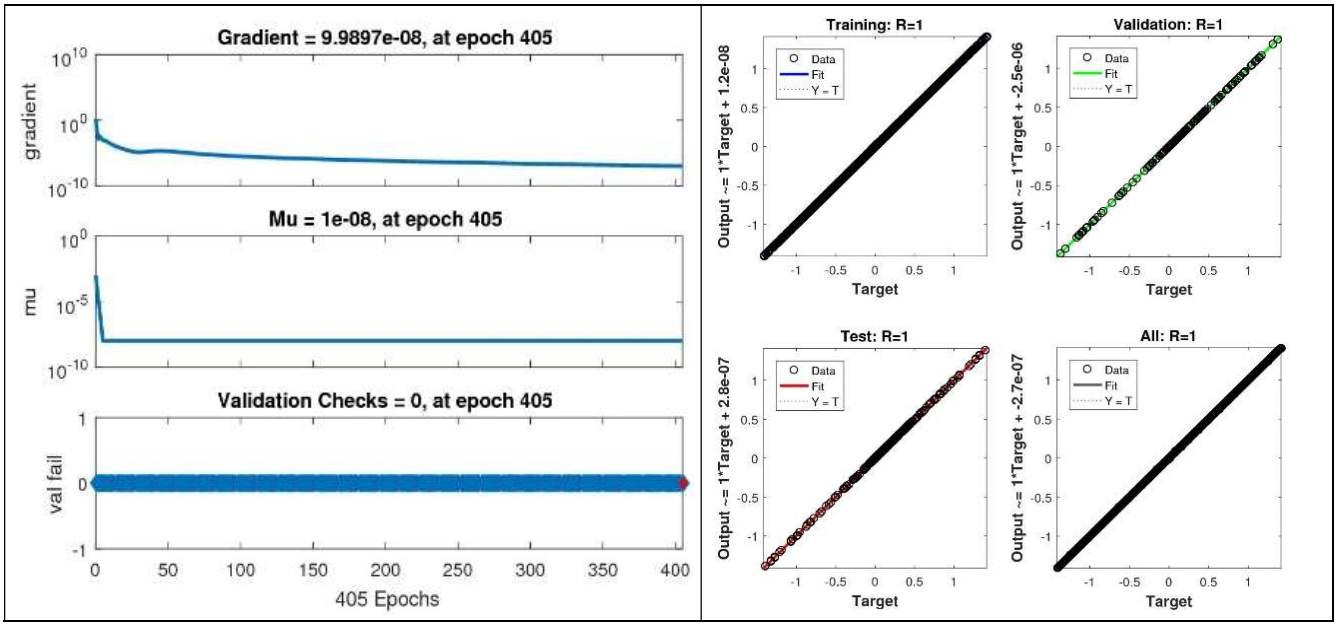

(c) State transition and regression analysis results for S3 of C4.

Figure 6(i). Proposed BPLMT-NN state transition and regression efficiency to solve the MHD-VNRD model for Scenarios 1–3 of Case 4.

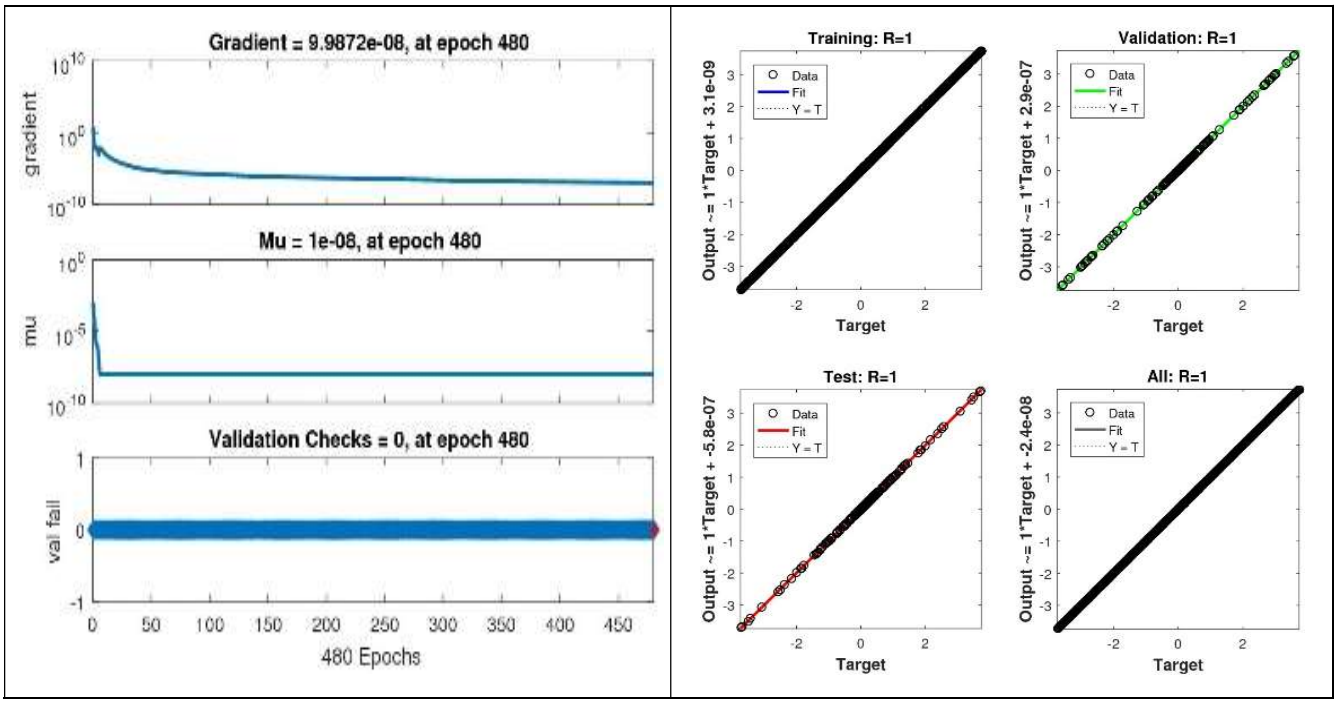

(a) State transition and regression analysis results for S4 of C4.

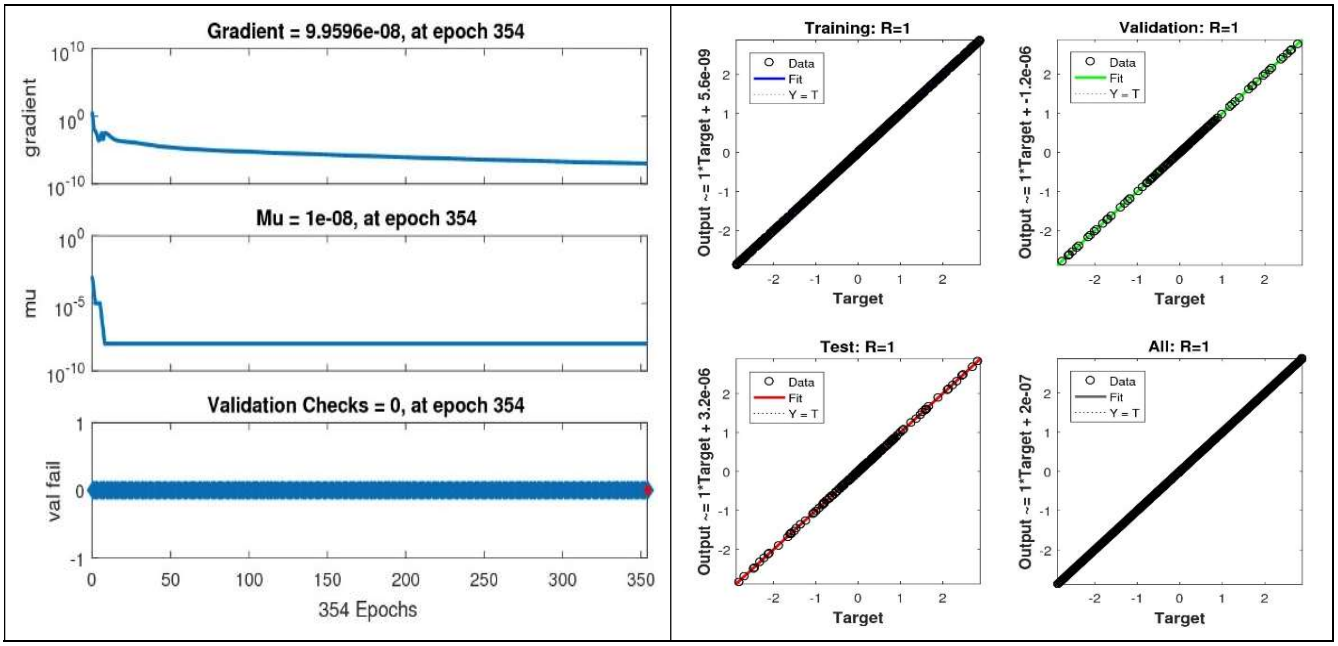

(b) State transition and regression analysis results for S5 of C4.

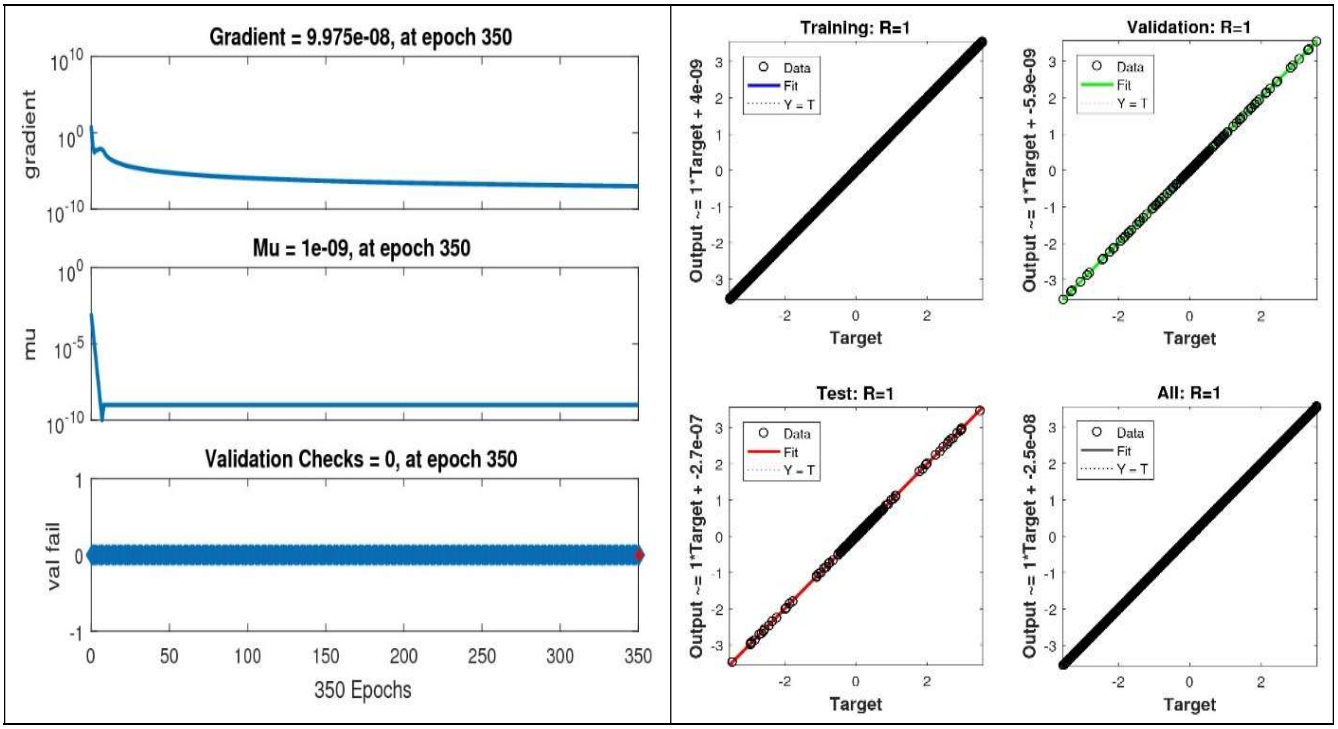

(c) State transition and regression analysis results for S6 of C4.

Figure 6(ii). Proposed BPLMT-NN state transition and regression efficiency to solve the MHD-VNRD model for Scenarios 4–6 of Case 4.

For the temperature profile $\theta(\eta)$), concentration $\phi(\eta)$, and radial and tangential velocities $f'(\eta)$ and $g(\eta)$, the BPLMT-NN effects are confirmed. They are shown in Figures 7(i) and 7(ii), respectively, for each of the six MHD-VNRD framework scenarios. Subfigures 7(i)(a,b,c) illustrate the impact of velocity profiles $f'(\eta)$, $g(\eta)$, and temperature profiles $\theta(\eta)$ on the fluctuation of Lewis number *Le*, magnetic parameter *M*, and velocity slip parameter γ for the MHD-VNRD model in

Scenarios 1–3. The impact of magnetic parameter *M* on the velocity profile f′(η) is seen in Figure 7(i)(a). For increasing values of the magnetic parameter, there is a reduction in both the velocity profile and the thickness of the momentum boundary layer. Higher values of the velocity slip parameter γ result in a lower velocity profile g(η) and a thinner momentum boundary layer, as seen in Figure 7(i)(b). This shows how a higher Lewis number Le results in a thinner concentration layer and a lower concentration profile ϕ(η). In light of this, the temperature profile $\theta(\eta)$ and concentration ϕ(η) for Scenarios 4–6 in the MHD-VNRD model are represented by different values in Subfigures 7(ii)(a,b,c), for the Brownian motion parameter *Nb*, thermophoresis parameter *Nt,* and Prandtl number *Pr*, respectively. The effect of the parameter *Nb* for Brownian motion on the temperature profile θ(η) is seen in Figure 7(ii)(a). When the bigger values of the Brownian motion parameter are taken into consideration, it is found that an improvement occurs in the temperature profile. Greater temperature and thermal boundary layer thickness are produced by larger Brownian motion parameters, which also have lesser viscous forces and greater Brownian diffusion coefficients. The impact of the thermophoresis parameter *Nt* on the concentration profile ϕ(η) is seen in Figure 7(ii)(b). Concentration profile and matching concentration layer thickness both grow in relation to the values of the thermophoresis parameters in this case. To make matters worse, increasing the thermophoretic force makes things worse by physically trying to stimulate the migration of nanoparticles in the opposite direction as the temperature gradient, which means that the concentration gradient is larger and the concentration profiles are less uniform. As seen in Figure 7(ii)(c), a decreased temperature profile θ(η) is caused by the Prandtl number *Pr*. It demonstrates that a decreasing temperature profile θ(η) and decreasing thermal boundary layer thickness are caused by a growing Prandtl number *Pr*. The Prandtl number is physically dependent on the diffusivity of heat. A lower thermal diffusivity is correlated with larger Prandtl numbers. The temperature profile and corresponding thickness of the thermal boundary layer decrease as a result of this reduced thermal diffusivity.

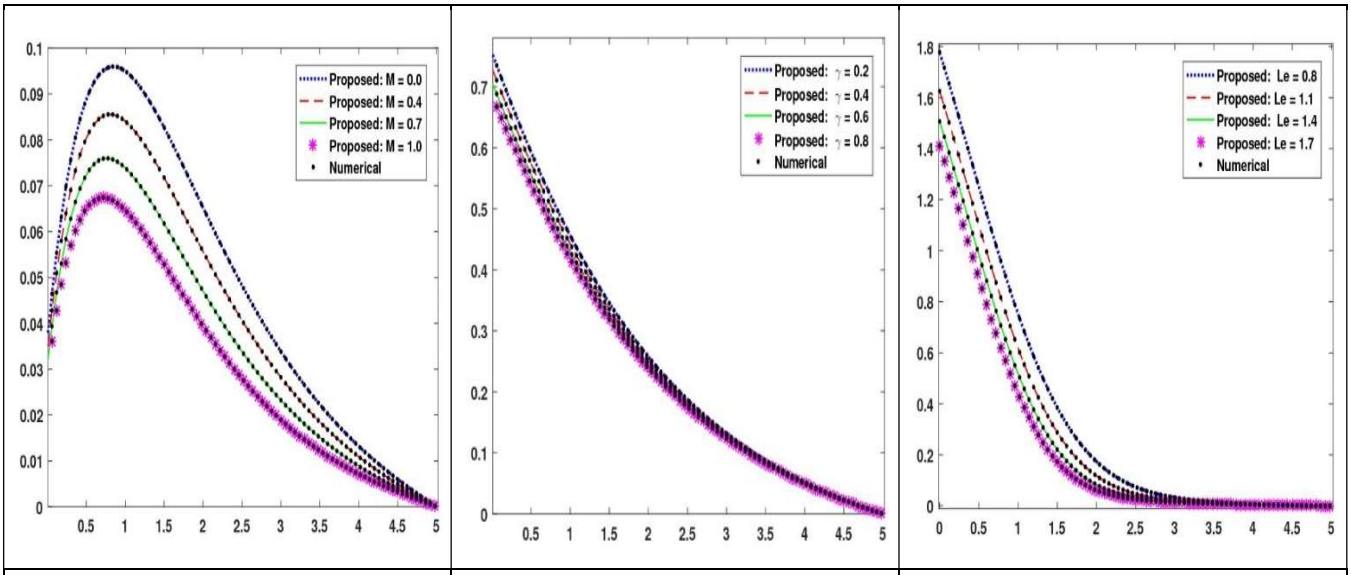

(a) Influence of M on $f'(\eta)$ | (b) Influence of γ on $g(\eta)$ | (c) Influence of Le on $\phi(\eta)$

Figure 7(i). Evaluation of suggested numerical consequences with recommended BLMS-ANNs Scenarios 1–3 of the MHD-VNRD model.

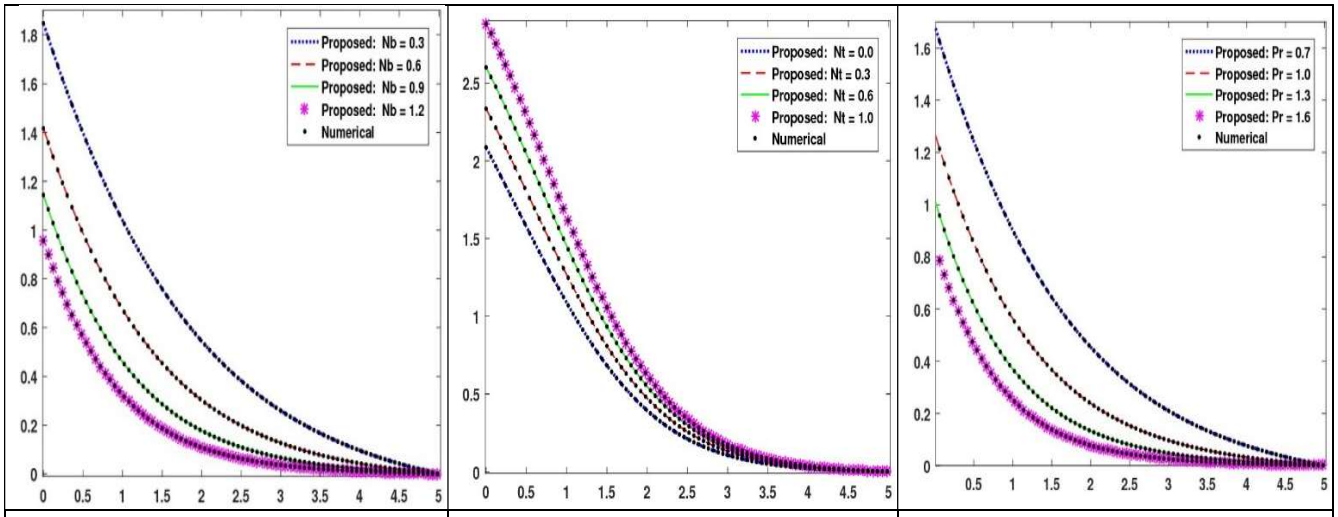

(a) Influence of Nb on $\theta(\eta)$ | (b) Influence of Nt on $\phi(\eta)$ | (c) Influence of Pr on $\theta(\eta)$

Figure 7(ii). Evaluation of suggestion numerical consequences with recommended BLMS-ANNs for Scenarios 4–6 of the MHD-VNRD model.

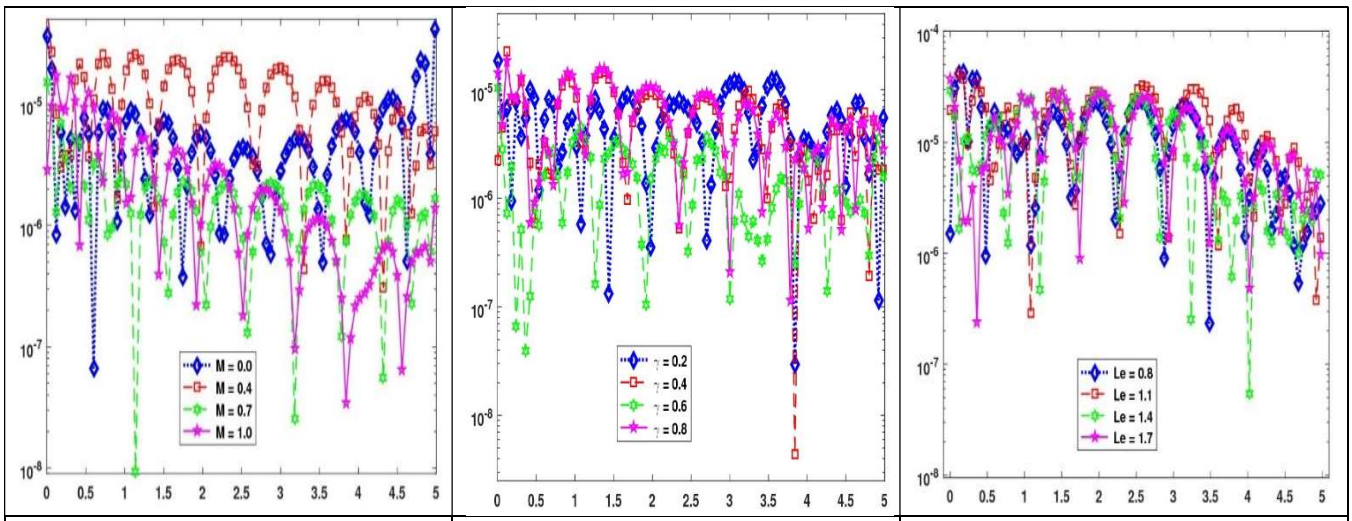

(a) AE of M on $f'(\eta)$ | (b) AE of γ on $g(\eta)$ | (c) AE of Le on $\phi(\eta)$

Figure 8(i). Suggested BPLMT-NN evaluation includes findings of absolute error analysis of the reference set of data for the MHD-VNRD model in Scenarios 1–3.

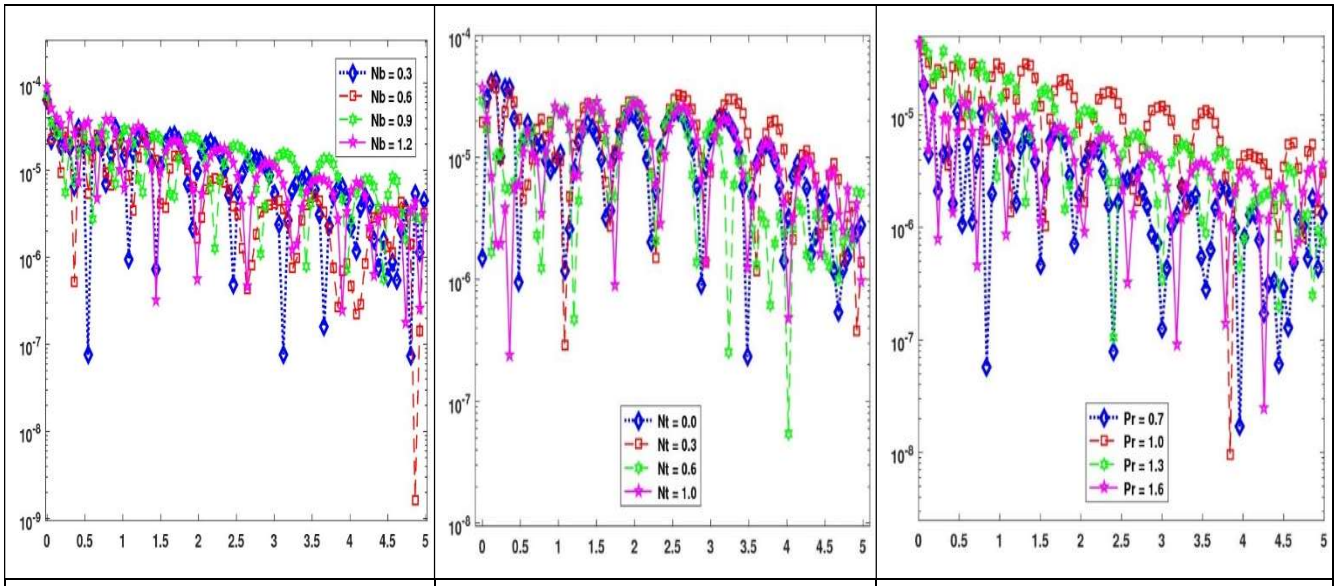

(a) AE of Nb on $\theta(\eta)$ | (b) AE of Nt on $\phi(\eta)$ | (c) AE of Pr on $\theta(\eta)$

Figure 8(ii). Suggested BPLMT-NN evaluation includes findings of absolute error analysis of the reference set of data for the MHD-VNRD model in Scenarios 4–6.

4. Conclusions

The magnetohydrodynamic investigation of the boundary layer flow of a viscous nanofluid due to the rotation of a disk under velocity slip conditions is carried out. Properties of heat transfer and mass are investigated when thermophoresis and Brownian motion are present. The backpropagation Levenberg-Marquardt approach combined with neural networks (BPLMT-NN) yields numerical solutions. The important facts of the current study are stated as follow:

- Higher magnetic parameter values decrease velocity distributions, while temperature and concentration distributions exhibit the reverse tendency.
- The backpropagation Levenberg-Marquardt technique with neural networks (BPLMT-NN) has been used to examine the solution of a mathematical model that displays the slip effect with modifications of certain situations or scenarios.
- By using relevant connected variables, a mathematical flow could be translated into a structure of nonlinear ODEs, which can be represented by PDEs.
- The explicit Runge-Kutta technique has been utilized to produce the dataset for the (MHD-VNRD) model.
- The deviations from several physical data, including the chemical reaction factor, velocity slip parameter, Prandtl number, magnetic field, thermophoresis, and Brownian motion and parameters, were included.
- Both of the velocity's components decrease as the velocity slip parameter increases.
- The distributions of concentration and temperature improve as the thermophoresis parameter increases.
- A number of variants of the MHD-VNRD reference data set are altered utilizing the BPLMT-NN for training, testing, and validation, using 80%, 10%, and 10% of the data set, respectively.

- ❖ The scheme's brilliance receives a 10^{-9} to 10^{-11} grade for both reference and suggested results.
- ❖ The functionality that has been explained is bolstered by both numerical and graphical depictions of regression dynamics, mean square errors, and convergence error-histogram graphs.

Future applications of the BPLMT-NN concept and its most recent improved versions might be in fluid dynamics problems [55–56] and a variety of computer network propagation models [57–58].

Author contributions

Yousef Jawarneh: Conceptualization, writing-review and editing, project administration; Samia Noor: Visualization, writing-review and editing, data curation, funding; Ajed Akbar: Data curation, project administration; Rafaqat Ali Khan: Resources, validation; Ahmad Shafee: Software, investigation, resources. All authors have read and agreed to the published version of the manuscript.

Use of Generative-AI tools declaration

The authors declare they have not used Artificial Intelligence (AI) tools in the creation of this article.

Funding

This work was supported by the Deanship of Scientific Research, Vice Presidency for Graduate Studies and Scientific Research, King Faisal University, Saudi Arabia [Grant No. KFU251494].

Conflict of interest

The authors declare that they have no conflicts of interest.

References

1. D. B. Parker, A comparison of algorithms for neuron-like cells, *AIP Conf. Proc.*, **151** (1986), 327–332. https://doi.org/10.1063/1.36233
2. A. Akbar, H. Ullah, M. A. Z. Raja, K. S. Nisar, S. Islam, M. Shoaib, A design of neural networks to study MHD and heat transfer in two phase model of nano-fluid flow in the presence of thermal radiation, *Wave. Random Complex*, 2022, 1–24. https://doi.org/10.1080/17455030.2022.2152905
3. M. Shoaib, M. A. Z. Raja, M. T. Sabir, S. Islam, Z. Shah, P. Kumam, et al., Numerical investigation for rotating flow of MHD hybrid nanofluid with thermal radiation over a stretching sheet, *Sci. Rep.*, **10** (2020), 1–15. https://doi.org/10.1038/s41598-020-75254-8
4. R. A. Khan, H. Ullah, M. A. Z. Raja, M. A. R. Khan, S. Islam, M. Shoaib, Heat transfer between two porous parallel plates of steady nanofluids with Brownian and Thermophoretic effects: A new stochastic numerical approach, *Int. Commun. Heat Mass Transf.*, **126** (2021), 105436. https://doi.org/10.1016/j.icheatmasstransfer.2021.105436
5. Z. Sabir, M. A. Z. Raja, J. L. Guirao, M. Shoaib, Integrated intelligent computing with neuro-swarming solver for multi-singular fourth-order nonlinear Emden–Fowler equation, *Comput. Appl. Math.*, **39** (2020), 1–18. https://doi.org/10.1007/s40314-020-01330-4

6. A. Shafiq, A. B. Çolak, T. N. Sindhu, Modeling of Soret and Dufour's convective heat transfer in nanofluid flow through a moving needle with artificial neural network, *Arab. J. Sci. Eng.*, **48** (2023), 2807–2820. https://doi.org/10.1007/s13369-022-06945-9
7. M. Shoaib, R. A. Khan, H. Ullah, K. S. Nisar, M. A. Z. Raja, S. Islam, et al., Heat transfer impacts on maxwell nanofluid flow over a vertical moving surface with MHD using stochastic numerical technique via artificial neural networks, *Coatings*, **11** (2021), 1483. https://doi.org/10.3390/coatings11121483
8. A. Akbar, H. Ullah, M. A. Z. Raja, S. Islam, K. S. Nisar, M. Shoaib, Intelligent networks for MHD fluid flow in a thermally stratified medium between coaxial stretchable rotating disks, *Wave. Random Complex*, 2023, 1–22. https://doi.org/10.1080/17455030.2023.2193852
9. T. N. Sindhu, A. B. Çolak, S. A. Lone, A. Shafiq, Reliability study of generalized exponential distribution based on inverse power law using artificial neural network with Bayesian regularization, *Qual. Reliab. Eng. Int.*, **39** (2023), 2398–2421. https://doi.org/10.1016/j.triboint.2023.108544
10. R. Lin, Q. Zhou, X. Nan, T. Hu, A parallel optimization method for robustness verification of deep neural networks, *Mathematics*, **12** (2024), 1884. https://doi.org/10.3390/math12121884
11. D. D. Ganji, M. Azimi, Application of DTM on MHD Jeffery Hamel problem with nanoparticle, *UPB Sci. Bull. Ser. A*, **75** (2013), 223–230.
12. F. Garoosi, G. Bagheri, M. M. Rashidi, Two phase simulation of natural convection and mixed convection of the nanofluid in square cavity, *Powder Technol.*, **275** (2015), 239–256. https://doi.org/10.1016/j.powtec.2015.02.013
13. M. K. Nayak, N. S. Akbar, V. S. Pandey, Z. H. Khan, D. Tripathi, 3D free convective MHD flow of nanofluid over permeable linear stretching sheet with thermal radiation, *Powder Technol.*, **315** (2017), 205–215. https://doi.org/10.1016/j.powtec.2017.04.017
14. S. U. Choi, J. A. Eastman, *Enhancing thermal conductivity of fluids with nanoparticles*, ANL/MSD/CP-84938; CONF-951135-29, Argonne National Laboratory, IL, 1995.
15. M. Sheikholeslami, T. Hayat, A. Alsaedi, MHD free convection of Al_2O_3–water nanofluid considering thermal radiation: A numerical study, *Int. J. Heat Mass Tran.*, **96** (2016), 513–524. https://doi.org/10.1016/j.ijheatmasstransfer.2016.01.059
16. M. M. Syam, M. Alkhedher, M. I. Syam, Thermal and hydrodynamic analysis of MHD nanofluid flow over a permeable stretching surface in porous media: Comparative study of Fe_3O_4, Cu, and Ag nanofluids, *Int. J. Thermofluids*, **26** (2025), 101055. https://doi.org/10.1016/j.ijft.2025.101055
17. O. D. Makinde, W. A. Khan, Z. H. Khan, Buoyancy effects on MHD stagnation point flow and heat transfer of a nanofluid past a convectively heated stretching/shrinking sheet, *Int. J. Heat Mass Tran.*, **62** (2013), 526–533. https://doi.org/10.1016/j.ijheatmasstransfer.2013.03.049
18. M. M. Bhatti, M. M. Rashidi, Numerical simulation of entropy generation on MHD nanofluid towards a stagnation point flow over a stretching surface, *Int. J. Appl. Comput. Math.*, **3** (2017), 2275–2289. https://doi.org/10.1007/s40819-016-0193-4
19. W. Ibrahim, B. Shankar, M. M. Nandeppanavar, MHD stagnation point flow and heat transfer due to nanofluid towards stretching sheet, *Int. J. Heat Mass Tran.*, **56** (2013), 1–9. https://doi.org/10.1016/j.ijheatmasstransfer.2012.08.034
20. M. M. Syam, M. I. Syam, Investigation of slip flow dynamics involving Al_2O_3 and Fe_3O_4 nanoparticles within a horizontal channel embedded with porous media, *Int. J. Thermofluids*, **24** (2024), 100934. https://doi.org/10.1016/j.ijft.2024.100934

21. S. Nadeem, S. Ahmad, N. Muhammad, Computational study of Falkner-Skan problem for a static and moving wedge, *Sensors Actuat. B-Chem.*, **263** (2018), 69–76. https://doi.org/10.1016/j.snb.2018.02.039
22. T. Von Karman, Uber laminare and turbulente Reibung, *Z. Angew. Math. Mech.*, **1** (1921), 233–252. https://doi.org/10.1002/zamm.19210010401
23. M. Turkyilmazoglu, P. Senel, Heat and mass transfer of the flow due to a rotating rough and porous disk, *Int. J. Therm. Sci.*, **63** (2013), 146–158. https://doi.org/10.1016/j.ijthermalsci.2012.07.013
24. M. M. Rashidi, N. Kavyani, S. Abelman, Investigation of entropy generation in MHD and slip flow over a rotating porous disk with variable properties, *Int. J. Heat Mass Tran.*, **70** (2014) 892–917. https://doi.org/10.1016/j.ijheatmasstransfer.2013.11.058
25. M. Turkyilmazoglu, Nanofluid flow and heat transfer due to a rotating disk, *Comput. Fluids*, **94** (2014), 139–146. https://doi.org/10.1016/j.compfluid.2014.02.009
26. K. Sharma, N. Vijay, F. Mabood, I. A. Badruddin, Numerical simulation of heat and mass transfer in magnetic nanofluid flow by a rotating disk with variable fluid properties, *Int. Commun. Heat Mass Tran.*, **133** (2022), 105977. https://doi.org/10.1016/j.icheatmasstransfer.2022.105977
27. M. Mustafa, J. A. Khan, T. Hayat, A. Alsaedi, On Bödewadt flow and heat transfer of nanofluids over a stretching stationary disk, *J. Mol. Liq.*, **211** (2015) 119–125. https://doi.org/10.1016/j.molliq.2015.06.065
28. M. Sheikholeslami, M. Hatami, D. D. Ganji, Numerical investigation of nanofluid spraying on an inclined rotating disk for cooling process, *J. Mol. Liq.*, **211** (2015) 577–583. https://doi.org/10.1016/j.molliq.2015.07.006
29. J. C. Maxwell, *A treatise on electricity and magnetism*, 2Eds., Clarendon Press, Oxford, UK, 1873.
30. K. B. Pavlov, Magnetohydrodynamic flow of an incompressible viscous fluid caused by deformation of a plane surface, *Magn. Gidrodin.*, **4** (1974), 146–147.
31. A. Chakrabarti, A. S. Gupta, Hydromagnetic flow and heat transfer over a stretching sheet, *Q. Appl. Math.*, **37** (1979) 73–78. Available from: https://www.ams.org/journals/qam/1979-37-01/S0033-569X-1979-99636-6/S0033-569X-1979-99636-6.pdf.
32. T. Hayat, T. Muhammad, S. A. Shehzad, A. Alsaedi, On three-dimensional boundary layer flow of Sisko nanofluid with magnetic field effects, *Adv. Powder Technol.*, **27** (2016) 504–512. https://doi.org/10.1016/j.apt.2016.02.002
33. S. Heysiattalab, A. Malvandi, D. D. Ganji, Anisotropic behavior of magnetic nanofluids (MNFs) at filmwise condensation over a vertical plate in presence of a uniform variable-directional magnetic field, *J. Mol. Liq.*, **219** (2016), 875–882. https://doi.org/10.1016/j.molliq.2016.04.004
34. T. Hayat, A. Aziz, T. Muhammad, A. Alsaedi, On magnetohydrodynamic three-dimensional flow of nanofluid over a convectively heated nonlinear stretching surface, *Int. J. Heat Mass Tran.*, **100** (2016), 566–572. https://doi.org/10.1016/j.ijheatmasstransfer.2016.04.113
35. T. Hayat, M. Waqas, M. I. Khan, A. Alsaedi, Analysis of thixotropic nanomaterial in a doubly stratified medium considering magnetic field effects, *Int. J. Heat Mass Tran.*, **102** (2016) 1123–1129. https://doi.org/10.1016/j.ijheatmasstransfer.2016.06.090
36. A. Malvandi, A. Ghasemi, D. D. Ganji, Thermal performance analysis of hydromagnetic Al_2O_3-water nanofluid flows inside a concentric microannulus considering nanoparticle migration and asymmetric heating, *Int. J. Therm. Sci.*, **109** (2016), 10–22. https://doi.org/10.1016/j.ijthermalsci.2016.05.023

37. T. Hayat, T. Muhammad, S. A. Shehzad, A. Alsaedi, An analytical solution for magnetohydrodynamic Oldroyd-B nanofluid flow induced by a stretching sheet with heat generation/absorption, *Int. J. Therm. Sci.*, **111** (2017), 274–288. https://doi.org/10.1016/j.ijthermalsci.2016.08.009
38. S. S. Motsa, P. G. Dlamini, M. Khumalo, Spectral relaxation method and spectral quasilinearization method for solving unsteady boundary layer flow problems, *Adv. Math. Phys.*, 2014, 1–12. https://doi.org/10.1155/2014/341964
39. S. Liao, On the homotopy analysis method for nonlinear problems, *Appl. Math. Comput.*, **147** (2004), 499–513. https://doi.org/10.1016/S0096-3003(02)00790-7
40. J. Wang, X. Ye, A weak Galerkin finite element method for second-order elliptic problems, *J. Comput. Appl. Math.*, **241** (2013), 103–115. https://doi.org/10.1016/j.cam.2012.10.003
41. N. M. Sarif, M. Z. Salleh, R. Nazar, Numerical solution of flow and heat transfer over a stretching sheet with Newtonian heating using the Keller box method, *Procedia Eng.*, **53** (2013), 542–554. https://doi.org/10.1016/j.proeng.2013.02.070
42. H. Ilyas, I. Ahmad, M. A. Z. Raja, M. B. Tahir, M. Shoaib, Intelligent computing for the dynamics of fluidic system of electrically conducting Ag/Cu nanoparticles with mixed convection for hydrogen possessions, *Int. J. Hydrogen Energ.*, **46** (2021), 4947–4980. https://doi.org/10.1016/j.ijhydene.2020.11.097
43. Z. Shah, M. A. Z. Raja, Y. M. Chu, W. A. Khan, S. Z. Abbas, M. Shoaib, et al., Computational intelligence of Levenberg-Marquardt backpropagation neural networks to study the dynamics of expanding/contracting cylinder for Cross magneto-nanofluid flow model, *Phys. Scr.*, **96** (2021), 055219. https://doi.org/ 10.1088/1402-4896/abe068
44. M. Awais, M. A. Z. Raja, S. E. Awan, M. Shoaib, H. M. Ali, Heat and mass transfer phenomenon for the dynamics of Casson fluid through porous medium over shrinking wall subject to Lorentz force and heat source/sink, *Alex. Eng. J.*, **60** (2021), 1355–1363. https://doi.org/10.1016/j.aej.2020.10.056
45. M. Umar, Z. Sabir, M. A. Z. Raja, M. Shoaib, M. Gupta, Y. G. Sánchez, A stochastic intelligent computing with neuro-evolution heuristics for nonlinear SITR system of novel COVID-19 dynamics, *Symmetry*, **12** (2020), 1628. https://doi.org/10.3390/sym12101628
46. T. N. Cheema, M. A. Z. Raja, I. Ahmad, S. Naz, H. Ilyas, M. Shoaib, Intelligent computing with Levenberg–Marquardt artificial neural networks for nonlinear system of COVID-19 epidemic model for future generation disease control, *Eur. Phys. J. Plus*, **135** (2020), 1–35. https://doi.org/10.1140/epjp/s13360-020-00910-x
47. A. Ali, S. U. Ilyas, S. Garg, M. Alsaady, K. Maqsood, R. Nasir, et al., Dynamic viscosity of Titania nanotubes dispersions in ethylene glycol/water-based nanofluids: Experimental evaluation and predictions from empirical correlation and artificial neural network, *Int. Commun. Heat Mass Transfer*, **118** (2020), 104882. https://doi.org/10.1016/j.icheatmasstransfer.2020.104882
48. M. Umar, M. A. Z. Raja, Z. Sabir, A. S. Alwabli, M. Shoaib, A stochastic computational intelligent solver for numerical treatment of mosquito dispersal model in a heterogeneous environment, *Eur. Phys. J. Plus*, **135** (2020), 1–23. https://doi.org/10.1140/epjp/s13360-020-00557-8
49. I. Jadoon, A. Ahmed, A. Rehman, M. Shoaib, M. A. Z. Raja, Integrated meta-heuristics finite difference method for the dynamics of nonlinear unipolar electro hydrodynamic pump flow model, *Appl. Soft Comput.*, **97** (2020), 106791. https://doi.org/10.1016/j.asoc.2020.106791
50. S. E. Awan, M. A. Z. Raja, F. Gul, Z. A. Khan, A. Mehmood, M. Shoaib, Numerical computing paradigm for investigation of micropolar nanofluid flow between parallel plates system with impact of electrical MHD and Hall current, *Arab. J. Sci. Eng.*, **46** (2021), 645–662. https://doi.org/10.1007/s13369-020-04736-8

51. Z. Sabir, M. Umar, J. L. Guirao, M. Shoaib, M. A. Z. Raja, Integrated intelligent computing paradigm for nonlinear multi-singular third-order Emden–Fowler equation, *Neural Comput. Appl.*, **33** (2021), 3417–3436. https://doi.org/10.1007/s00521-020-05187-w
52. I. Ahmad, M. A. Z. Raja, H. Ramos, M. Bilal, M. Shoaib, Integrated neuro-evolution-based computing solver for dynamics of nonlinear corneal shape model numerically, *Neural Comput. Appl.*, **33** (2021), 5753–5769. https://doi.org/10.1007/s00521-020-05355-y
53. F. Faisal, M. Shoaib, M. A. Z. Raja, A new heuristic computational solver for nonlinear singular Thomas–Fermi system using evolutionary optimized cubic splines, *Eur. Phys. J. Plus*, **135** (2020), 1–29. https://doi.org/10.1140/epjp/s13360-019-00066-3
54. T. Hayat, T. Muhammad, S. A. Shehzad, A. Alsaedi, On magnetohydrodynamic flow of nanofluid due to a rotating disk with slip effect: A numerical study, *Comput. Method. Appl. Mech. Eng.*, **315** (2017), 467–477. https://doi.org/10.1016/j.cma.2016.11.002
55. M. Awais, S. E. Awan, M. A. Z. Raja, M. Shoaib, Effects of gyro-tactic organisms in bio-convective nano-material with heat immersion, stratification, and viscous dissipation, *Arab. J. Sci. Eng.*, **46** (2021), 5907–5920. https://doi.org/10.1007/s13369-020-05070-9
56. M. Sheikholeslami, M. B. Gerdroodbary, R. Moradi, A. Shafee, Z. Li, Application of neural network for estimation of heat transfer treatment of Al_2O_3-H_2O nanofluid through a channel, *Comput. Methods Appl. Mech. Eng.*, **344** (2019), 1–12. https://doi.org/10.1016/j.cma.2018.09.025
57. Z. Sabir, D. Baleanu, M. Shoaib, M. A. Z. Raja, Design of stochastic numerical solver for the solution of singular three-point second-order boundary value problems, *Neural Comput. Appl.*, **33** (2021), 2427–2443. https://doi.org/10.1007/s00521-020-05143-8
58. Z. Sabir, M. A. Z. Raja, J. L. G. Guirao, M. Shoaib, A novel design of fractional Meyer wavelet neural networks with application to the nonlinear singular fractional Lane-Emden systems, *Alex. Eng. J.*, **60** (2021), 2641–2659. https://doi.org/10.1016/j.aej.2021.01.004

AIMS Press